ACSNANO

www.acsnano.org

ARTICLE

Graphene-Sealed Flow Cells for *In Situ* Transmission Electron Microscopy of Liquid Samples

Gabriel Dunn,[▽] Vivekananda P. Adiga,[▽] Thang Pham, Christopher Bryant, Donez J. Horton-Bailey, Jason N. Belling, Ben LaFrance, Jonathan A. Jackson, Hamid Reza Barzegar, Jong Min Yuk, Shaul Aloni, Michael F. Crommie, and Alex Zettl*

Cite This: *ACS Nano* 2020, 14, 9637–9643

Read Online

ACCESS | Metrics & More | Article Recommendations | Supporting Information

ABSTRACT: **We introduce a graphene-based nanofluidic cell that facilitates *in situ* imaging of liquid samples via transmission electron microscopy. The cell combines the benefits of graphene liquid cells—namely, high resolution, reduced charging effects, and excellent sample stability—with the ability to introduce reactants and control fluid concentrations as provided by conventional silicon-nitride-windowed flow cells. The graphene flow cell offers significantly less window bowing compared to existing commercial holders. We demonstrate the performance of the flow cell by imaging gold nanoparticle dynamics and uranyl acetate crystallization. Our results confirm the utility of graphene flow cells in obtaining the high spatial and temporal resolution required for probing the complex dynamics of nanoparticles and nucleation pathways in aqueous solutions.**

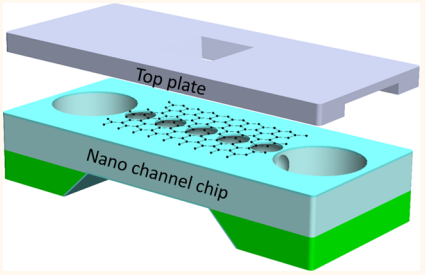

KEYWORDS: *graphene liquid cells, liquid cell transmission electron microscopy, flow cells, resolution, nanofluidic channel*

Transmission electron microscopy (TEM) is an invaluable tool for the study of nanoscale systems. While transmission electron microscopes invariably operate under high-vacuum conditions, sealed insertion cells allow the study of diverse liquid samples at atmospheric pressure and room temperature. Nanoparticles are often produced and/or dispersed in solution, critical biological reactions typically take place at the nanoscale entirely in solution, and even macroscopic phenomena such as mineral crystallization begin as nanoscale nucleation events in liquid environment. While optical microscopy is severely limited in resolving nanoscopic systems, aberration-corrected TEM can yield single-atom resolution. However, TEM of liquid samples presents a number of challenges.[1−4] The cell windows and liquid itself scatter electrons, requiring the windows and liquid layer in the cell to be kept as thin as possible. On the other hand, windows must be robust enough to withstand liquid/vacuum interface stresses without rupture.[2]

Although *in situ* liquid TEM was demonstrated soon after the development of TEM, the past two decades have witnessed a resurgence of interest in liquid cell TEM due to advances in microfabrication. Fluidic setups using silicon nitride (Si_3N_4) membranes have allowed the adaptation of standard TEM machines for *in situ* liquid experiments,[1,2,5,6] and commercial flow cells are readily available. This has facilitated the study of various phenomena including nanoparticle growth, nanoparticle dissolution and dynamics,[7,8] salt precipitation,[9] nanoelectrochemistry,[10] and biological systems.[5] Despite these successes, Si_3N_4-based liquid cells have drawbacks: the Si_3N_4 window thickness required for structural stability can compromise achievable resolution,[11] electron beam irradiation of the Si_3N_4 causes charging effects, and high-energy electrons can induce significant sample damage. In addition, the standard assembly method of sandwiching two nitride membrane chips results in significant outward bowing of the windows,[10,12] further increasing the overall thickness of the surrounding liquid.

Graphenic enclosure of the bacteria on silicon nitride has been demonstrated by Mohanty et al., where reduced charging effects enabled cell wall imaging.[13] Yuk et al.[7] demonstrated graphene as an encapsulating material for *in situ* liquid-based TEM. By entrapping a solution between two atomically thin sheets of graphene, the growth of Pt nanocrystals was imaged

Received: January 16, 2020
Accepted: July 28, 2020
Published: July 28, 2020

https://dx.doi.org/10.1021/acsnano.0c00431
ACS Nano 2020, 14, 9637–9643

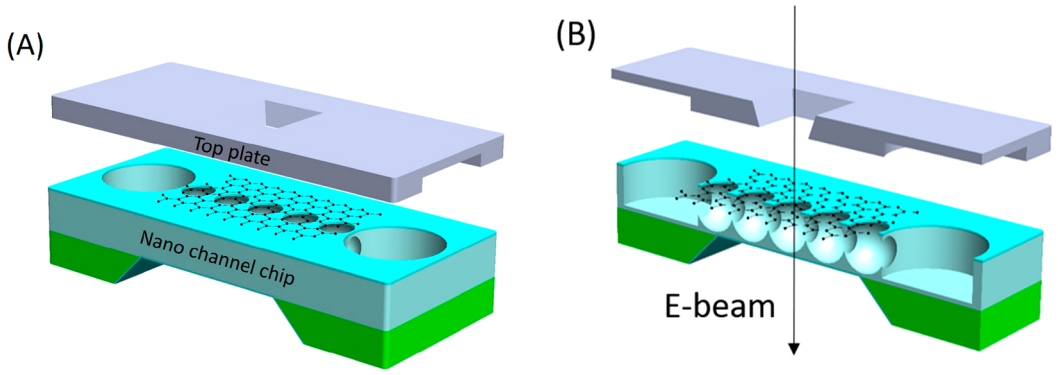

Figure 1. Schematic representation of major components of the graphene flow cell (GFC). (A) Shows the unassembled nanochannel chip and top plate. (B) Shows cross section. The GFC consists of a bottom chip with an integrated windowed nanochannel and a top plate, pressed over the nanochannel chip, which facilitates fluid flow connections. The bottom chip consists of a triple stackup of $Si_3N_4/SiO_2/Si_3N_4$. A series of overlapping and hence interconnected cavities within the SiO_2 layer forms the nanochannel. The series of smaller holes or apertures in the Si_3N_4 membrane covering the tops of each cavity is draped with graphene, yielding a series of electron-transparent graphene windows along the nanochannel. In this depiction of the GFC, the bottom windows of the cavities consist of extremely thin Si_3N_4, but graphene windows can also be utilized here. An indium film (not shown) serves as a sealing gasket when the top plate is mated to the nanochannel chip.

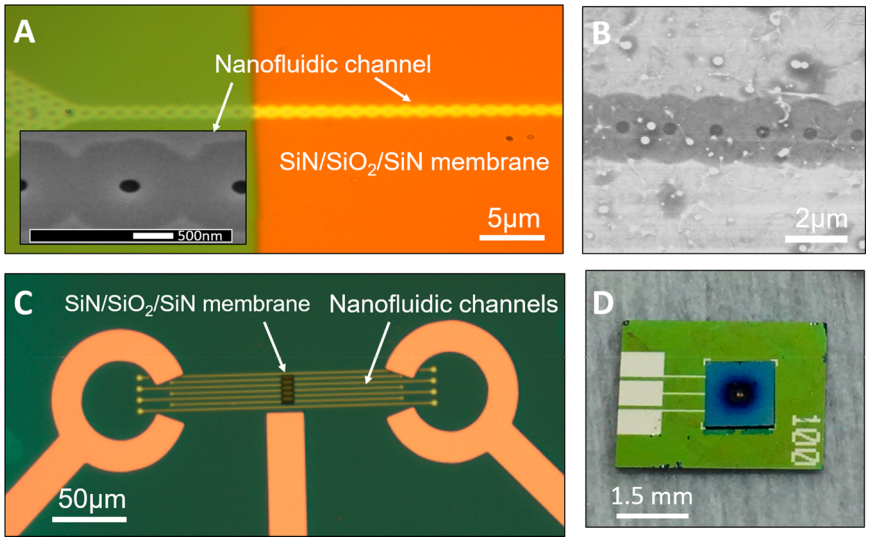

Figure 2. Optical and SEM images of GFC chips. (A) Optical image of nanofluidic channel formed by selectively etching SiO_2 sandwiched between Si_3N_4 (inset: SEM image of the nanopatterned holes in the top nitride film used as an etch mask for the underlying oxide, creating the interconnected cavities that form the nanochannel). The orange region is the $Si_3N_4/SiO_2/Si_3N_4$ suspended membrane, and the green region is where the stack is on a silicon substrate. (B) SEM image of graphene transferred over the nitride holes sealing the top of the nanochannel. (C) Bottom chip with multiple channels between Au electrodes passing through the $Si_3N_4/SiO_2/Si_3N_4$ suspended membrane (dark rectangular region in the center). (D) Optical image of fully assembled chip along with the top plate.

with atomic resolution, a significant improvement over previous methods utilizing conventional window liquid cells. Graphene presents several advantages as a window material: it is the thinnest and strongest possible encapsulating material,[13] it limits sample charging and radiation damage thanks to its excellent electrical conductivity,[13,14] and it can getter from the solution harmful oxidative radicals created by the electron beam.[15,16] Such radicals are especially detrimental to biological specimens.

All graphene-based liquid cells (GLC) reported to date have been static sealed cells that rely on evaporation to seal them during the assembly process. Some of these are cells wrapped in graphene and transferred onto silicon nitride windows, whereas the other rely on microwells in silicon nitride enclosed by graphene.[9,13,15−22] Because static cells are hermetically sealed, all reactants for a desired reaction must be present in the cell as it is being sealed; it is not possible to externally introduce or remove reactants or byproducts during imaging. While there has been some success in using the TEM electron beam itself to initiate reactions, the inability to introduce arbitrary chemical species, and thus to initiate reactions on-demand, severely limits its potential applications.[8] Furthermore, the reliance on evaporation to seal the graphene sheets to each other or to a substrate can result in highly variable chemical concentrations in the ultimately sealed sample, and final concentrations may differ dramatically from the initial or desired concentrations.

Herein, we demonstrate a graphene-windowed TEM liquid cell with integrated nanochannels, which we term the graphene flow cell (GFC).[23] The design combines the benefits of the

https://dx.doi.org/10.1021/acsnano.0c00431
ACS Nano 2020, 14, 9637−9643

Si_3N_4-based flow cell and the static graphene liquid cell. Importantly, the nanochannel width, depth, and length are all here precisely controlled, and fluid can be introduced into and removed from the channel, at will, during the experiment. The performance of the flow cell is demonstrated by imaging gold nanoparticle dynamics and uranyl acetate crystallization.

RESULTS/DISCUSSION

Figure 1a shows a simplified schematic of the GFC design. A bottom chip (formed from a monolithic $Si_3N_4/SiO_2/Si_3N_4$ stack) incorporates the nanofluidic channel with input and output ports, together with a series of circular viewing apertures along the top and bottom of the channel. The top apertures are always windowed with graphene (shown), while the bottom apertures are windowed with either graphene or ultrathin Si_3N_4 (in the experiments described below, the bottom windows are ultrathin Si_3N_4). The thicknesses of the Si_3N_4 (bottom), SiO_2, and Si_3N_4 (top) layers used here are 14, 75, and 7 nm, respectively. A top plate, ultimately mated to the bottom chip via an indium seal, facilitates external fluidic connection to the GFC. Figure 1b shows in perspective a cross-sectional view of the GFC. The nanochannel is formed from a series of lithographically defined and acid-etched overlapping and hence interconnected cavities, where the windows are located at the tops and bottoms of each of the hollow cavities. Although only one nanochannel is shown in the schematics of Figure 1(a,b); in practice many closely spaced parallel nanochannels are created in the bottom chip, connecting common input and output ports. This ensures that if one channel becomes inadvertently blocked, other channels can still function, and the experiment is not impaired. The fabrication process and assembly of the GFC components (bottom chip and top plate) is described in detail in the Supporting Information.

Figure 2 illustrates images of actual GFC devices. Figure 2A shows an SEM image of the nanochannel region. The interior width of the nanochannel is ~2 μm. The inset of Figure 2A shows a zoomed-in view of three cavities that make up part of the nanochannel. The darker gray contrast region identifies the interconnected cavities (each of diameter 2 μm) beneath the Si_3N_4 capping membrane. The black spots in the center of each cavity identify the holes (apertures) in the capping membrane, each of a diameter of ~200 nm. When covered with graphene, these become the top windows of the nanochannel. Figure 2B shows an SEM image of a nanochannel segment after graphene deposition; the row of six small dark dots running left to right across the image identifies the graphene windows. Figure 2C shows a somewhat zoomed-out optical microscope image of seven parallel nanochannels formed in the bottom nanochannel chip. The large orange "C" shaped objects at the left and right, and the orange vertical bar at center, are supplementary gold electrodes (not shown in Figure 1) that allow optional electrical biasing and electrochemistry to be performed before or during TEM imaging. The three independent electrodes address respectively the left and right fluid ports and the channel center. Figure 2D shows a photograph of the entire completed GFC.

It is worth emphasizing the advantages the GFC presents. Traditional flow cells typically rely on two thick Si_3N_4 membranes that act as top and bottom windows to separate flowing liquid samples from the high-vacuum environment of the TEM. As mentioned above, in the GFC, the top (or both top and bottom) Si_3N_4 windows are replaced by graphene. By integrating the channel onto a single chip and limiting the channel width to few microns ($\leq$2 μm), we avoid the window bowing issues seen in commercial chips. Because of undercutting during the acid etch for the nanochannel fabrication, the window apertures have a much smaller diameter than the cavity diameter beneath them, as was shown in Figures 1 and 2. This is highly advantageous, as the graphene is then required to span only the smaller holes and not the full channel width. Prior to using the device, we confirm by SEM imaging that the graphene properly seals all the holes along the nanochannel. The graphene windows serve multiple purposes: they easily and tightly seal the fluidic channel, they create multiple extremely thin, conducting viewing windows along the channel, and, as for GLCs, they serve as reactive ion getters. The GFC is, in effect, a GLC with more tightly controlled geometry (cell width, depth, and length), with the additional benefits of nanofluidic input and output. If the bottom Si_3N_4 windows are retained in the GFC, the narrow channel width allows ultrathin Si_3N_4 windows in the thickness range of 5−10 nm to be utilized, whereas commercial Si_3N_4-based cells typically employ 50 nm thick windows.

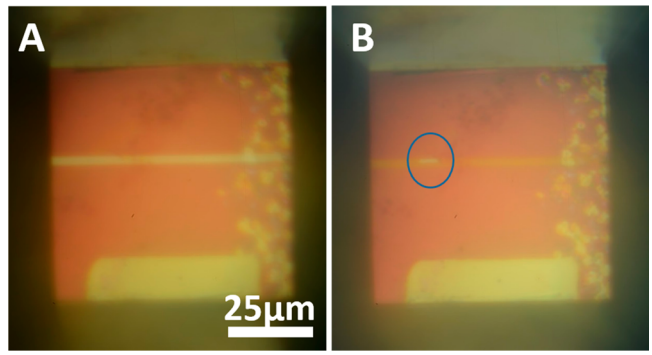

Figure 3. Wetting of nanochannel by pure deionized water. (A) Optical image of empty nanochannel taken in test setup. (B) Image taken after DI water has filled the nanochannel. A small trapped bubble is circled in blue. All images are to the same scale. Details of the optical imaging setup used to take these images are in the Supporting Information.

We first use the GFC to image the dynamics of gold nanoparticles (Au NPs) in solution. Owing to their high contrast and their commercial availability, metallic nanoparticles have been extensively studied by *in situ* liquid cell microscopy. Introducing AuNPs into the GFC allows us to demonstrate that new species in solution can be readily introduced into the nanochannel and confirms effective imaging of liquid-borne species within the TEM column. Pure deionized water (DI) is first introduced into the channel. The TEM electron beam is blanked in order to avoid bubble formation, and a phosphate buffered solution containing Au NPs is introduced into the fluidic port of the TEM holder. After approximately 5 min, AuNPs are observed via TEM in the channel. Due to the high impedance of the nanochannel, compared to the fluidic bypass around the port chip from the inlet to the outlet side, the AuNP introduction into the viewing area is dominated by diffusion. The ability to introduce new solutions and diffusively mix solutions in the nanochannel greatly increases the utility of the GFC for a variety of experiments.

https://dx.doi.org/10.1021/acsnano.0c00431
ACS Nano 2020, 14, 9637−9643

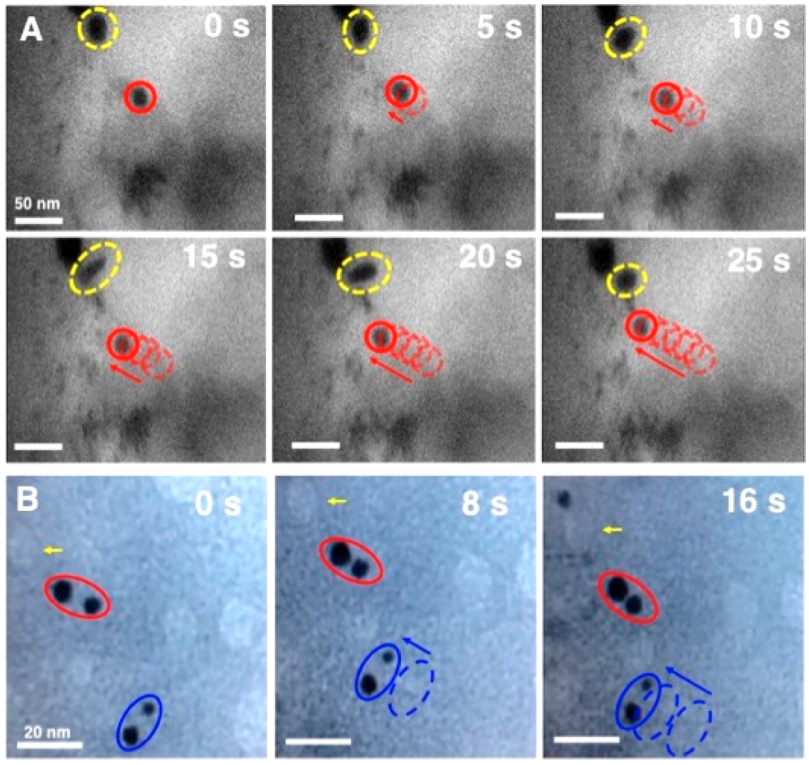

Figure 4. Au NP dynamics. (A) TEM time series of a gold nanoparticle (encircled by yellow-dashed line) rotating and a Au NP moving across the field of view (red lines: solid circle shows the current location, fainted dashed circles show previous positions; the red arrows indicate direction of the particle translation in time order). Images were taken in a GFC with a 100 nm thick viewing nanochannel, with 25 nm thick Si_3N_4 layers. Field of view is over the graphene covered holes in the top layer of Si_3N_4. (B) TEM time series of Au nanoparticle pairs in buffered solution. The first pair (top left) circled in red change their interparticle distance. The Au particles in the second pair (bottom) enclosed in blue maintain the same gap over the time of observation. Solid blue circles show the current position of the pair, while the dashed blue ones show the previous locations. The yellow arrow shows a contamination on the graphene window, which is used as the reference marker to deduce the translation of the blue pair. In (B), the false background color (blue) is applied to aid visualization.

Figure 4 shows dynamics of the Au NPs within the GFC obtained by TEM imaging. There are two distinct phenomena. First, we observe the shrinking and growing of a gold particle (particle #1, enclosed within a yellow-dashed line in the top left corner of all panels in Figure 4A). From 0 s (when we start recording the dynamics) to 10 s, the particle is slightly reduced in (projected) dimension, from approximately 469 to 440 nm^2. Simultaneously, the particle rotates about 15° clockwise (seen by referencing to the surrounding objects). Between the 10 and 15 s frames, the particle dramatically changes from a rounded shape to a rod-like one with negligible rotation. Between the 15−20 s frames, the particle again rotates clockwise for roughly 20° and then starts shrinking (presumably dissolving back into the solution) from 479 to 355 nm^2 in projected area, to a more rounded geometry, as ultimately seen in the 25 s frame. The yellow-dashed line shapes indicate qualitatively the projected geometry of the particle in the corresponding frames. A video of a representative NP dynamics is included in Supporting Movie 1.

The second phenomenon we track in our GFC is the movement of a gold nanoparticle (particle #2, marked with a red circle in the first (0 s) frame of Figure 4A). Over time, the particle does not change its dimension much, but instead, it executes discrete steps of motion. First, it apparently rotates about itself between the 0−10 s frames, after which it translates toward the bigger particle (particle #1). The trajectory of particle #2 is illustrated by red circles (the solid circle shows its position in the current frame and the dashed circles with fainted color show its locations in previous frames). The arrows show the direction of motion. For example, in the 10 s frame, the dashed circle shows its position in the previous frame (5 s frame), while the solid circle indicates its current position (10 s frame). The arrow shows the relationship (in time order) of the circles. Over the course of 25 s, the particle diffusively translates over a distance of approximately 68 nm, which makes the translational velocity of 2.7 nm/s for a single particle (the particle size is about 15 nm in diameter).

The attraction force and interaction between nanoparticles have been shown previously in other TEM liquid cell studies.[24] The translation and rotational speeds of Au NPs are significantly less than those predicted by the Einstein−Stokes equation.[15,24,25] Convective currents initiated by the beam appear to dominate the Au NP movements. 3D tracking of the nanoparticles is also possible, as height information can be inferred relative to the position of nanoparticles that are assumed to be in fixed contact with the windows. Figure 4B shows an example of gold particle pairwise translation and interaction observed in our GFC. For the first pair of gold nanoparticles, marked by a red circle, the two particles move closer to each other from the first frame to the second frame (from 5.0 to 1.5 nm), but they maintain the same gap over the next frame. More interestingly, the other pair of gold particles, enclosed by a blue line, maintains roughly the same interparticle distance over the course of observation (16 s) while translating together toward the first pair. The blue pair harmonically translate 19 nm over 16 s, which makes the

https://dx.doi.org/10.1021/acsnano.0c00431
ACS Nano 2020, 14, 9637−9643

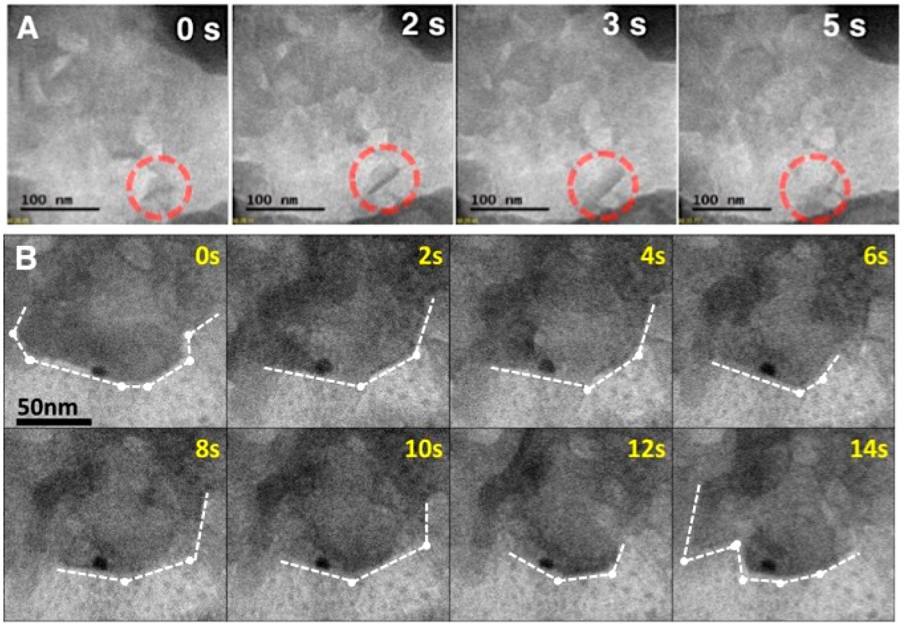

Figure 5. TEM images of uranyl acetate (UA) nanocrystals in the GFC. (A) Circled in red is a platelet rotating in the nanochannel. (B) UA nanocrystal morphology dynamics. Facets (bounded by white dashed lines) at the nanocrystal front can grow and shrink under electron beam irradiation.

translational velocity of 1.2 nm/s for a pair of particles. The solid blue line indicates the current position of the pair, while the dashed line shows the previous locations. The yellow arrow shows a contamination on the graphene membrane, which is used as a reference marker to align images in order to map the particles' movement in successive frames.

Our result confirms that the GFC provides high spatial and temporal resolution for imaging/tracking of complex dynamics of nanoparticles in an aqueous environment. We further note that, due to the limitations of using the commercial TEM holder in JEOL 2010 TEM operated at 80 keV as well as the finite thickness of the GFC, our resolution is limited compared to the static graphene cells imaged using a TEAM 0.5 microscope.[7]

As a second demonstration of GFC capabilities, we examine a uranyl acetate (UA) crystallization process. We combine 0.1% uranyl acetate solution with a dilute phosphate buffer solution. Phosphate is known to cause uranyl acetate to precipitate from solution, and exposure to UV light can also enhance the precipitation rate of uranyl crystals. We thus infer that the combination of dilute phosphate buffer solution and electron beam irradiation can initiate nucleation of uranyl crystals from solution. Figure 5 shows the formation of nanocrystal uranyl acetate platelets within the GFC. As highlighted in the TEM image time series of Figure 5A, we observe a distinct rotational movement of a UA crystal (at the bottom right corner of all frames and marked by a red-dashed circle). The plate-like UA crystallite undergoes a rotation about itself along its longitudinal axis, showing different facets of the same crystallite.

Figure 5B shows the structural transformation of a large UA crystal. In all frames, the shapes of the crystal are delineated by white-dashed lines. The dots indicate the corners of the facets enclosed the growing front of the crystal. At the 0 s frame, the initial geometry of the crystal is bounded by seven facets. Over a few seconds (from 0 to 6 s frames), while the facets at the bottom right corner were very stable against the beam damaging and beam-induced chemical dissolution, the facets on the left corner experience roughening. As a result, in the next 6 s (from the 8 to 14 s frames), the rough faces dissolve and gradually become irregular. This is because atoms at rough surfaces are assembled in a more disordered manner (high-energy state) and are thus removed more easily without a high-energy cost. Simultaneously, the facets on the bottom right still maintain a well-defined crystallographic orientation, evidenced by sharp angles (approximately 120−135°) at the corners. Our results illustrate the complex kinetics involved in crystal nucleation and growth and complement other liquid cell TEM studies. The experiments here again demonstrate the capability and versatility that the GFC offers in probing different nucleation pathways in liquid environments.

CONCLUSIONS

We have demonstrated the fabrication and application of the graphene flow cell (GFC), a graphene-sealed nanochannel cell for high-resolution *in situ* TEM imaging of liquid samples. The GFC is compatible with widely available commercial *in situ* liquid TEM specimen holders and presents significant improvements over existing liquid cells. We have demonstrated the GLC function for Au nanoparticle and uranyl acetate nanocrystal dynamics, and the technology is applicable to a wide variety of nanoscale systems in liquid. The inclusion of graphene as a viewing window brings the known benefits of the static GLC to dynamic nanofluidic cell imaging.

EXPERIMENTAL METHODS

For operation, the GFC assembly is loaded into a commercially available Protochips TEM holder, capable of introducing liquid samples via fluidic ports. Liquids are introduced by syringe pump through PEEK tubing and exit the holder through an outlet port. The liquid sample collects in a reservoir sealed from the vacuum of the TEM, allowing for diffusive flow through the nanochannel, while providing a bypass for flow past the nanochannel. Such a bypass is necessary, as the dimensions of the nanochannel would otherwise require significantly long time to achieve complete fluid exchange.

https://dx.doi.org/10.1021/acsnano.0c00431
ACS Nano 2020, 14, 9637−9643

Before the holder is inserted into the TEM, the initial liquid filling of the GFC nanochannel is monitored via optical microscopy to ensure there are no visible leaks or blockages. The channel is first filled with IPA at a rate of 50 μL/min. Filling of the channel is confirmed by a change in channel contrast and would typically occur in less than 5 min of pumping. We insert the Protochips TEM holder into a vacuum chamber and pump down to 10^{-6} Torr to confirm there are no leaks. For aqueous samples, DI water is then pumped through the TEM head stage for 15 min to replace the IPA by diffusive flow. Samples can be introduced prior to inserting the holder into the TEM or during imaging. No additional surface treatments are necessary in order to fill the channels, as illustrated in Figure 3. We remark that static GLCs are sometimes difficult to seal using DI water, presumably because of the hydrophobicity of graphene. This problem is overcome in the GFC with heterostructured windows, where a portion of the flow channel is made from silicon dioxide. The TEM holder, with GFC, is inserted into a JEOL 2010 TEM operated at 80 keV. We demonstrate operation of the GFC using two physical systems.

ASSOCIATED CONTENT

Supporting Information

The Supporting Information is available free of charge at https://pubs.acs.org/doi/10.1021/acsnano.0c00431.

Step by step fabrication process and assembly of graphene flow cell for *in situ* TEM imaging is described in detail; details of an optical setup used to capture images of the flow cell used in the article (PDF)

Supporting Movie 1: Representative video of nanoparticle dynamics (MP4)

AUTHOR INFORMATION

Corresponding Author

Alex Zettl − *Department of Physics, University of California at Berkeley, Berkeley, California 94720, United States; Materials Sciences Division, Lawrence Berkeley National Laboratory, Berkeley, California 94720, United States; Kavli Energy NanoSciences Institute at the University of California at Berkeley and the Lawrence Berkeley National Laboratory, Berkeley, California 94720, United States*; Email: azettl@berkeley.edu

Authors

Gabriel Dunn − *Department of Physics, University of California at Berkeley, Berkeley, California 94720, United States; Materials Sciences Division, Lawrence Berkeley National Laboratory, Berkeley, California 94720, United States; Kavli Energy NanoSciences Institute at the University of California at Berkeley and the Lawrence Berkeley National Laboratory, Berkeley, California 94720, United States*

Vivekananda P. Adiga − *Department of Physics, University of California at Berkeley, Berkeley, California 94720, United States; Materials Sciences Division, Lawrence Berkeley National Laboratory, Berkeley, California 94720, United States; Kavli Energy NanoSciences Institute at the University of California at Berkeley and the Lawrence Berkeley National Laboratory, Berkeley, California 94720, United States;* orcid.org/0000-0001-5979-6830

Thang Pham − *Department of Physics, University of California at Berkeley, Berkeley, California 94720, United States; Kavli Energy NanoSciences Institute at the University of California at Berkeley and the Lawrence Berkeley National Laboratory, Berkeley, California 94720, United States*

Christopher Bryant − *Department of Physics, University of California at Berkeley, Berkeley, California 94720, United States; Materials Sciences Division, Lawrence Berkeley National Laboratory, Berkeley, California 94720, United States; Kavli Energy NanoSciences Institute at the University of California at Berkeley and the Lawrence Berkeley National Laboratory, Berkeley, California 94720, United States*

Donez J. Horton-Bailey − *Department of Physics, University of California at Berkeley, Berkeley, California 94720, United States; Materials Sciences Division, Lawrence Berkeley National Laboratory, Berkeley, California 94720, United States; Kavli Energy NanoSciences Institute at the University of California at Berkeley and the Lawrence Berkeley National Laboratory, Berkeley, California 94720, United States*

Jason N. Belling − *Department of Physics, University of California at Berkeley, Berkeley, California 94720, United States*

Ben LaFrance − *Department of Biochemistry and Molecular Biology, University of California at Berkeley, Berkeley, California 94720, United States;* orcid.org/0000-0003-0229-5255

Jonathan A. Jackson − *Department of Physics, University of California at Berkeley, Berkeley, California 94720, United States;* orcid.org/0000-0001-5051-1499

Hamid Reza Barzegar − *Department of Physics, University of California at Berkeley, Berkeley, California 94720, United States; Materials Sciences Division, Lawrence Berkeley National Laboratory, Berkeley, California 94720, United States; Kavli Energy NanoSciences Institute at the University of California at Berkeley and the Lawrence Berkeley National Laboratory, Berkeley, California 94720, United States;* orcid.org/0000-0002-1314-5407

Jong Min Yuk − *Department of Physics, University of California at Berkeley, Berkeley, California 94720, United States; Materials Sciences Division, Lawrence Berkeley National Laboratory, Berkeley, California 94720, United States; Kavli Energy NanoSciences Institute at the University of California at Berkeley and the Lawrence Berkeley National Laboratory, Berkeley, California 94720, United States;* orcid.org/0000-0002-4677-7363

Shaul Aloni − *The Molecular Foundry, Lawrence Berkeley National Laboratory, Berkeley, California 94720, United States*

Michael F. Crommie − *Department of Physics, University of California at Berkeley, Berkeley, California 94720, United States; Kavli Energy NanoSciences Institute at the University of California at Berkeley and the Lawrence Berkeley National Laboratory, Berkeley, California 94720, United States;* orcid.org/0000-0001-8246-3444

Complete contact information is available at: https://pubs.acs.org/10.1021/acsnano.0c00431

Author Contributions

$^{\nabla}$G.D. and V.P.A. contributed equally to the manuscript.

Notes

The authors declare no competing financial interest.

ACKNOWLEDGMENTS

This work was supported primarily by the U.S. Department of Energy, Office of Science, Office of Basic Energy Sciences, Materials Sciences and Engineering Division under Contract No. DE-AC02-05-CH11231, under the Nanomachines Program (KC1203), which provided for construction of the GFC

https://dx.doi.org/10.1021/acsnano.0c00431
ACS Nano 2020, 14, 9637−9643

and TEM testing with gold nanocrystals. Support is also acknowledged from the National Science Foundation under Grant No. DMR-1807233, which provided for uranyl acetate experiments. The Defense Threat Reduction Agency (DTRA) under award HDTRA1-13-1-0035 supported early GFC design concepts. The authors acknowledge Martin Sandberg for help with image rendering of the flow cell and Frances Ross and Shu Fen Tan for helpful discussions.

REFERENCES

(1) Williamson, M. J.; Tromp, R. M.; Vereecken, P. M.; Hull, R.; Ross, F. M. Dynamic Microscopy of Nanoscale Cluster Growth at the Solid-Liquid Interface. *Nat. Mater.* **2003**, *2*, 532−536.
(2) Ross, F. M., Ed. *Liquid Cell Electron Microscopy*; Cambridge University Press: Cambridge, U.K., 2016.
(3) Ross, F. M. Opportunities and Challenges in Liquid Cell Electron Microscopy. *Science* **2015**, *350*, No. aaa9886.
(4) Liao, H.-G.; Zheng, H. Liquid Cell Transmission Electron Microscopy. *Annu. Rev. Phys. Chem.* **2016**, *67*, 719−747.
(5) Peckys, D. B.; de Jonge, N. Visualizing Gold Nanoparticle Uptake in Live Cells with Liquid Scanning Transmission Electron Microscopy. *Nano Lett.* **2011**, *11*, 1733−1738.
(6) de Jonge, N.; Peckys, D. B.; Kremers, G. J.; Piston, D. W. Electron Microscopy of Whole Cells in Liquid with Nanometer Resolution. *Proc. Natl. Acad. Sci. U. S. A.* **2009**, *106*, 2159−2164.
(7) Yuk, J. M.; Park, J.; Ercius, P.; Kim, K.; Hellebusch, D. J.; Crommie, M. F.; Lee, J. Y.; Zettl, A.; Alivisatos, A. P. High-Resolution EM of Colloidal Nanocrystal Growth Using Graphene Liquid Cells. *Science* **2012**, *336*, 61−64.
(8) Ye, X.; Jones, M. R.; Frechette, L. B.; Chen, Q.; Powers, A. S.; Ercius, P.; Dunn, G.; Rotskoff, G. M.; Nguyen, S. C.; Adiga, V. P.; Zettl, A.; Rabani, E.; Geissler, P. L.; Alivisatos, A. P. Single-Particle Mapping of Nonequilibrium Nanocrystal Transformations. *Science* **2016**, *354*, 874−877.
(9) Sasaki, Y.; Kitaura, R.; Yuk, J. M.; Zettl, A.; Shinohara, H. Efficient Preparation of Graphene Liquid Cell Utilizing Direct Transfer with Large-Area Well-Stitched Graphene. *Chem. Phys. Lett.* **2016**, *650*, 107−112.
(10) Holtz, M. E.; Yu, Y.; Gunceler, D.; Gao, J.; Sundararaman, R.; Schwarz, K. A.; Arias, T. A.; Abruña, H. D.; Muller, D. A. Nanoscale Imaging of Lithium Ion Distribution During *In Situ* Operation of Battery Electrode and Electrolyte. *Nano Lett.* **2014**, *14*, 1453−1459.
(11) de Jonge, N.; Houben, L.; Dunin-Borkowski, R. E.; Ross, F. M. Resolution and Aberration Correction in Liquid Cell Transmission Electron Microscopy. *Nat. Rev. Mater.* **2019**, *4*, 61−78.
(12) Holtz, M. E.; Yu, Y.; Gao, J.; Abruña, H. D.; Muller, D. A. *In Situ* Electron Energy-Loss Spectroscopy in Liquids. *Microsc. Microanal.* **2013**, *19*, 1027−1035.
(13) Mohanty, N.; Fahrenholtz, M.; Nagaraja, A.; Boyle, D.; Berry, V. Impermeable Graphenic Encasement of Bacteria. *Nano Lett.* **2011**, *11*, 1270−1275.
(14) Keskin, S.; de Jonge, N. Reduced Radiation Damage in Transmission Electron Microscopy of Proteins in Graphene Liquid Cells. *Nano Lett.* **2018**, *18*, 7435−7440.
(15) Chen, Q.; Smith, J. M.; Park, J.; Kim, K.; Ho, D.; Rasool, H. I.; Zettl, A.; Alivisatos, A. P. 3D Motion of DNA-Au Nanoconjugates in Graphene Liquid Cell Electron Microscopy. *Nano Lett.* **2013**, *13*, 4556−4561.
(16) Cho, H.; Jones, M. R.; Nguyen, S. C.; Hauwiller, M. R.; Zettl, A.; Alivisatos, A. P. The Use of Graphene and Its Derivatives for Liquid-Phase Transmission Electron Microscopy of Radiation-Sensitive Specimens. *Nano Lett.* **2017**, *17*, 414−420.
(17) Rasool, H.; Dunn, G.; Fathalizadeh, A.; Zettl, A. Graphene-Sealed Si/SiN Cavities for High-Resolution *In Situ* Electron Microscopy of Nano-Confined Solutions. *Phys. Status Solidi B* **2016**, *253*, 2351−2354.
(18) Hutzler, A.; Schmutzler, T.; Jank, M. P. M.; Branscheid, R.; Unruh, T.; Spiecker, E.; Frey, L. Unravelling the Mechanisms of Gold-Silver Core-Shell Nanostructure Formation by *In Situ* TEM Using an Advanced Liquid Cell Design. *Nano Lett.* **2018**, *18*, 7222−7229.
(19) Shin, D.; Park, J. B.; Kim, Y.-J.; Kim, S. J.; Kang, J. H.; Lee, B.; Cho, S.-P.; Hong, B. H.; Novoselov, K. S. Growth Dynamics and Gas Transport Mechanism of Nanobubbles in Graphene Liquid Cells. *Nat. Commun.* **2015**, *6*, 6068.
(20) Textor, M.; De Jonge, N. Strategies for Preparing Graphene Liquid Cells for Transmission Electron Microscopy. *Nano Lett.* **2018**, *18*, 3313−3321.
(21) Kelly, D. J.; Zhou, M.; Clark, N.; Hamer, M. J.; Lewis, E. A.; Rakowski, A. M.; Haigh, S. J.; Gorbachev, R. V. Nanometer Resolution Elemental Mapping in Graphene-Based TEM Liquid Cells. *Nano Lett.* **2018**, *18*, 1168−1174.
(22) Park, J.; Park, H.; Ercius, P.; Pegoraro, A. F.; Xu, C.; Kim, J. W.; Han, S. H.; Weitz, D. A. Direct Observation of Wet Biological Samples by Graphene Liquid Cell Transmission Electron Microscopy. *Nano Lett.* **2015**, *15*, 4737−4744.
(23) Adiga, V. P.; Dunn, G.; Zettl, A. K.; Alivisatos, A. P. Liquid Flow Cells Having Graphene on Nitride for Microscopy. US 9449787 B2, 2016.
(24) Verch, A.; Pfaff, M.; de Jonge, N. Exceptionally Slow Movement of Gold Nanoparticles at a Solid/Liquid Interface Investigated by Scanning Transmission Electron Microscopy. *Langmuir* **2015**, *31*, 6956−6964.
(25) Tuteja, A.; Mackay, M. E.; Narayanan, S.; Asokan, S.; Wong, M. S. Breakdown of the Continuum Stokes-Einstein Relation for Nanoparticle Diffusion. *Nano Lett.* **2007**, *7*, 1276−1281.

https://dx.doi.org/10.1021/acsnano.0c00431
ACS Nano 2020, 14, 9637−9643